Bond order wave instabilities in doped frustrated antiferromagnets:
"Valence bond solids" at fractional filling

M. Indergand,[1] A. Läuchli,[2] S. Capponi,[3] and M. Sigrist[1]

[1] *Theoretische Physik, ETH-Hönggerberg, CH-8093 Zürich*
[2] *Institut Romand de Recherche Numérique en Physique des Matériaux (IRRMA), EPFL, CH-1015 Lausanne*
[3] *Laboratoire de Physique Théorique, CNRS UMR 5152, Université Paul Sabatier, F-31062 Toulouse*
(Dated: February 6, 2008)

We explore both analytically and numerically the properties of doped $t-J$ models on a class of highly frustrated lattices, such as the kagomé and the pyrochlore lattice. Focussing on a particular sign of the hopping integral and antiferromagnetic exchange, we find a generic symmetry breaking instability towards a twofold degenerate ground state at a fractional filling below half filling. These states show modulated bond strengths and only break lattice symmetries. They can be seen as a generalization of the well-known valence bond solid states to fractional filling.

I. INTRODUCTION

Highly frustrated quantum magnets are fascinating and complex systems where the macroscopic ground state degeneracy at the classical level leads to many intriguing phenomena at the quantum level. The ground state properties of spin $S = 1/2$ Heisenberg antiferromagnets on the kagomé and the pyrochlore lattice remain still puzzling and controversial in many aspects. While the magnetic properties of the Heisenberg and extended models have indeed been studied for quite some time, the investigation of highly frustrated magnets upon doping with mobile charge carriers has started recently[1-6]. Such interest has been motivated for example by the observation that in some strongly correlated materials, such as the spinel compound LiV_2O_4, itinerant charge carriers and frustrated magnetic fluctuations interact strongly[7]. Furthermore the possibility of creating optical kagomé lattices in the context of cold atomic gases has been pointed out[8], making it possible to "simulate" interacting fermionic or bosonic models in an artificial setting[9].

At this point we should stress that the behavior in a simple single-band model at weak and at strong correlations are not expected to be related in a trivial way. The weak coupling limit allows us to discuss the electronic properties within the picture of itinerant electrons in momentum space based on the notions of a Fermi surface and Fermi surface instabilities (see e.g. Refs. 1,4). Considering for example the Fermi surfaces of a triangular or a kagomé lattice at half filling we do not find any obvious signature of the magnetic frustration present at large U. Although at weak coupling these systems do not seem to be particularly special, at intermediate to strong coupling the high density of low-energy fluctuations of the highly frustrated systems display characteristic features from which the physics of the frustrated system of localized degrees of freedom will emerge[2,3].

In the following we study a class of highly frustrated lattices, the so called bisimplex lattices[10], which are composed of corner-sharing simplices residing on a bipartite underlying lattice. We restrict ourselves to the triangle and the tetrahedron as the basic building blocks in the following. This class hosts lattices such as the kagomé or the pyrochlore lattice.

Our main result is the spontaneous symmetry breaking between the simplices, that are located on different sublattices of the underlying bipartite lattice. This instability takes place at the electron density $n = 2/3$ for the triangle based lattices like the kagomé lattice and at the density $n = 1/2$ for the tetrahedron based lattices like the pyrochlore lattice and leads to a bond order wave (BOW) phase where the kinetic energy is staggered for the neighboring simplices. This instability is driven by a cooperative effect of the kinetic energy *and* the exchange interactions.

The outline of the paper is the following: In Sec. II we introduce the lattices and the model and provide general arguments for the occurrence of the spontaneous symmetry breaking. These arguments are based on the analysis of the spectrum of isolated simplices and on a doped quantum dimer model. We then report in Sec. III mean-field calculations for the kagomé and the pyrochlore lattices which underline the symmetry breaking tendency. In Sec. IV we present numerical results for the kagomé lattice, that were obtained by exact diagonalization (ED) and by the contractor renormalization algorithm (CORE). In Sec. V the 1D analogue of the kagomé lattice, the so-called kagomé strip, is treated with two powerful methods that are available for 1D systems: the density matrix renormalization group (DMRG) and a fermionic renormalization group (RG) and bosonization analysis. Finally we summarize and conclude in Sec. VI.

II. GENERAL MOTIVATION

The bisimplex lattices shown in Fig. 1 consist of corner-sharing simplices (triangles or tetrahedra) that are located on an underlying bipartite lattice. Therefore, we can separate the triangles and the tetrahedra into two different classes, which is visualized in Fig. 1 by a different line-style (light and bold bonds). To refer to the simplices of a given class we call them "up"- and "down"-simplices, and we use the same terminology to distinguish
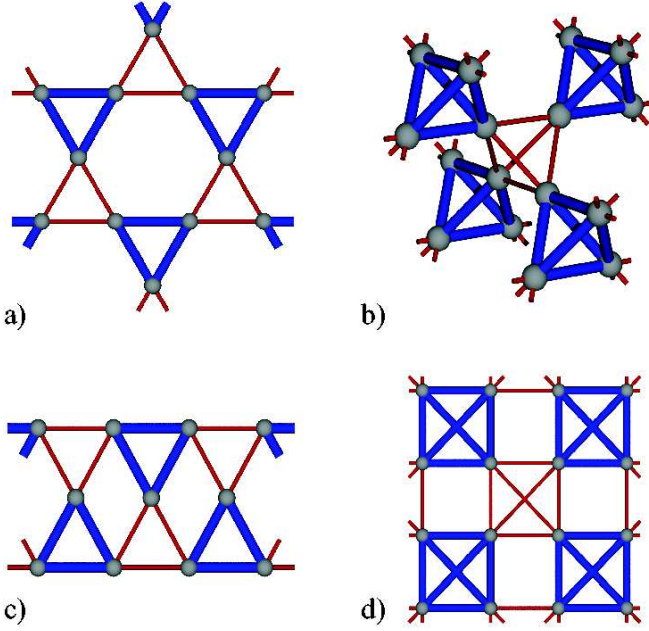
N_e	triangle Energy	Degen.		tetrahedron Energy	Degen.
0	0	1×1		0	1×1
1	$-2t$	1×2	*	$-3t$	1×2
	t	2×2		t	3×2
2	$-2t - J$	1×1	*	$-4t - J$	1×1
	$t - J$	2×1		$-J$	3×1
	$-t$	2×3	*	$2t - J$	2×1
	$2t$	1×3		$-2t$	3×3
				$2t$	3×3
3	$-3J/2$	2×2	*	$-2t - 3J/2$	3×2
	0	1×4		$-3J/2$	2×2
				$2t - 3J/2$	3×2
				$-t$	3×4
				$3t$	1×4
4				$-3J$	2×1
				$-2J$	3×3
				0	1×5

FIG. 1: (Color online) Four different bisimplex-lattices. The kagomé lattice (a) and the pyrochlore lattice (b) together with their lower dimensional analogues, the kagomé strip (c) and the checkerboard lattice (d). The two types of corner sharing units ("up" vs "down") are distinguished by the line width. They correspond to the bond order wave symmetry breaking pattern occurring at $n = 2/3$ on the triangle based lattices and at $n = 1/2$ on the tetrahedron based lattices.

TABLE I: Classification of the eigenstates of the $t-J$ model on a triangle and on a tetrahedron. The degeneracy is given in the form $r \times (2S + 1)$, where r is the dimension of the irreducible representation of $\mathcal{S}_3$, respectively $\mathcal{S}_4$, and S is the total spin of the state. The asterix denotes the states retained in the CORE calculations for the kagomé system, see text.

the triangles, the tetrahedra or the lattice bonds.

In this section we provide two different arguments why for correlated electrons on such lattices at the fractional filling with two electrons per "up"-simplex (one electron per simplex) a spontaneous symmetry breaking can be expected, resulting in a phase where the "up"-simplices differ from the "down"-simplices. For the kagomé and the pyrochlore lattice the inversion symmetry is broken in this phase, whereas for the lower-dimensional analogues, the kagomé strip and the checkerboard lattice, translational symmetry is broken. The following two arguments apply generally to all bisimplex lattices shown in Fig. 1. They are simple and illustrate the basic underlying physics. In the remaining sections we will provide detailed numerical and analytical evidence for several of these bisimplex lattices, which show that these arguments provide the correct picture. In the following we use (unless otherwise specified) the $t-J$ model to describe the correlated electrons on these lattices. The $t-J$ Hamiltonian is given by

$$\hat{H}_{t-J} = -t \sum_{\langle ij \rangle} \sum_{\sigma} \mathcal{P}(c_{i\sigma}^{\dagger} c_{j\sigma} + \text{h.c.}) \mathcal{P} \qquad (1)$$
$$+ J \sum_{\langle ij \rangle} (\mathbf{S}_i \cdot \mathbf{S}_j - \frac{1}{4} n_i n_j),$$

where the restriction to the subspace of singly occu-

pied sites is enforced by the projection operator $\mathcal{P} = \prod_i (1 - n_{i\uparrow} n_{i\downarrow})$. The hopping amplitude t is always chosen to be positive. A negative sign of t will most likely induce ferromagnetic tendencies at the fillings we are considering[11].

A. The limit of decoupled simplices

To get a basic understanding of the effect of doping in highly frustrated lattices we first consider the limit of decoupled simplices by turning the couplings within the "down"-simplices off. To connect this limit with the uniform lattice we use the parameter α ($0 \leq \alpha \leq 1$) that tunes the coupling strength of the "down"-bonds as $(\alpha t, \alpha J)$, while the coupling strength on the "up"-bonds is kept constant at (t, J). For $\alpha < 1$ the inversion symmetry between the "up"- and the "down"-simplices is explicitly broken by the Hamiltonian. The eigenvalues of $\hat{H}_{t-J}$ and their degeneracies are listed in Table I for a single triangle and a single tetrahedron. For $t > 0$ and $J \geq 0$, there is a non-degenerate state with $N_e = 2$ that has the lowest energy of all states and is separated from the remaining spectrum by a finite gap. This state has at the same time the lowest kinetic energy ($-2t$ or $-4t$, respectively) of all states and gains the maximal exchange energy ($-J$) for two spins. This state is not frustrated anymore because it minimizes the kinetic and the exchange energy at the same time. After having revealed

this particularly stable state with two electrons on a single unit, we know that for $\alpha = 0$ the system with two electrons per "up"-simplex has a non-degenerate ground state and a finite gap to all excitations. In the tight-binding model the gap decreases with increasing α and vanishes exactly at $\alpha = 1$. For interacting electrons, however, the strong correlations that are induced by the constraint in the kinetic term of the $t-J$ model and the frustration of the exchange term, that arises from the strong frustration of the lattice, are accompanied by a tendency to occupy rather local states (in our case, they still keep a substantial part of their kinetic energy) and to pair up the electrons in nearest neighbor singlets. Therefore, it is a reasonable possibility that the system even for $\alpha = 1$ has a finite gap and breaks the symmetry between the "up"- and the "down"-simplices spontaneously in order to profit from the bipartite and non-frustrated structure of the underlying lattice. Such an instability has the character of a bond order wave – i.e., modulated expectation values of the bond energies – and yields an insulating state which breaks inversion or translational symmetry, respectively.

B. Doped quantum dimer model

In the previous sections we considered the case $\alpha = 0$, where the Hamiltonian itself is not invariant under inversion symmetry. In order to get some insight into the mechanism of spontaneous symmetry breaking, it is desirable to treat "up"- and "down"-simplices on equal footing. In the following, we present a simple but illustrative model with a symmetric Hamiltonian that breaks spontaneously the symmetry between the "up"- and "down"-simplices in the ground state.

A close inspection of the wavefunction of the lowest energy eigenstate of two electrons on either a triangle or a tetrahedron reveals that it consists of the equal amplitude superposition of all possible positions of the singlet formed by the two electrons:

$$|\psi_{GS}\rangle = \frac{1}{\mathcal{N}} \sum_{i<j} (c_{i,\uparrow}^{\dagger} c_{j,\downarrow}^{\dagger} - c_{i,\downarrow}^{\dagger} c_{j,\uparrow}^{\dagger})|0\rangle, \qquad (2)$$

where the normalization $\mathcal{N} = \sqrt{3}$ for the triangle and $\mathcal{N} = \sqrt{6}$ for the tetrahedron. This wavefunction motivates us to design a simple quantum dimer model which on each triangle prefers the exact wavefunction described above. Such a Hamiltonian reads for example for the kagomé lattice:

$$
\begin{aligned}
H_{\text{QDM}} &= -t \sum_{\triangle} \left[|\triangle\rangle\langle\triangle| + |\triangle\rangle\langle\triangle| + |\triangle\rangle\langle\triangle| + \text{h.c.} \right] \\
&\quad -t \sum_{\nabla} \left[|\nabla\rangle\langle\nabla| + |\nabla\rangle\langle\nabla| + |\nabla\rangle\langle\nabla| + \text{h.c.} \right] (3)
\end{aligned}
$$

where the Hilbert space consists of all coverings of the kagomé lattice with N_c nearest-neighbor dimers and N_c

monomers, N_c counting the number of unit cells. This corresponds to the situation at $n = 2/3$ in the $t-J$ model. The interpretation is simple: the antiferromagnetic exchange term favors all the electrons to pair up into singlets, while the kinetic energy term delocalizes the singlets on a triangle. The quantum dimer model for the tetrahedron based lattices are defined by letting a single singlet resonate on a tetrahedron. This simple model allows us to find the exact ground state on these lattices. The ground state is twofold degenerate and each state is the direct product of equal amplitude resonances on the same type of triangles/tetrahedra, either all "up" or all "down". In such a situation each resonating dimer can independently fully optimize its kinetic energy. The argument has much in common with the reasoning for the close packed dimer model on the pyrochlore lattice discussed in Ref. 12.

Although this model is only a cartoon version of the real electronic system, it illustrates how the tendency of the electrons to form nearest-neighbor singlets obstructs the motion of the singlets between corner-sharing simplices, but within a given simplex an individual singlet can hop without obstacles and optimize its kinetic energy. The bipartite nature of the underlying lattice allows for the localization of the singlets on simplices without interference and triggers in this way the spontaneous symmetry breaking.

III. MEAN-FIELD DISCUSSION

In this section we present a mean-field calculation for the kagomé lattice and the pyrochlore lattice. The mean-field discussion is particularly valuable for the pyrochlore lattice, as due to its higher dimension it is less affected by fluctuations and is presently not treatable with numerical methods. We can show that in the mean-field analysis the spontaneous inversion symmetry breaking, discussed in the previous sections, is also the natural and leading instability.

We start with discussing the properties of the nearest-neighbor tight-binding model on the kagomé and the pyrochlore lattice, given by

$$\hat{H}_0 = -\mu\hat{N} - t \sum_{\mathbf{r},\sigma} \sum_{m \neq n} \sum_{\nu=\pm 1} c_{\mathbf{r}+\nu\mathbf{a}_m,\sigma}^{\dagger} c_{\mathbf{r}+\nu\mathbf{a}_n,\sigma}, \qquad (4)$$

where $\sigma \in \{\uparrow,\downarrow\}$ is the spin index and the indices m,n run from zero to the dimension of the lattice, d. Furthermore, $\mathbf{r}$ is an elementary lattice vector connecting unit cells and the vectors $\mathbf{a}_0,\ldots,\mathbf{a}_d$ point to the vertices of an elementary triangle (tetrahedron) in the kagomé (pyrochlore) lattice, $\mathbf{a}_0 = 0$. $\hat{N}$ is the total electron number operator and μ is the chemical potential. In the following we will use units where $t = 1$ and we will always choose $\mu = -1$ for the kagomé and $\mu = -2$ for the pyrochlore lattice, which corresponds to two electrons per unit cell. $\hat{H}_0$ can be diagonalized in reciprocal space and can be

written as

$$\hat{H}_0 = \sum_{\mathbf{k},m,\sigma} \xi_{\mathbf{k}m} \gamma^{\dagger}_{\mathbf{k}m\sigma} \gamma_{\mathbf{k}m\sigma}, \qquad (5)$$

with

$$-\xi_{\mathbf{k}0} = \xi_{\mathbf{k}1} \equiv \xi_{\mathbf{k}}, \quad \xi_{\mathbf{k}m} = d+1 \text{ for } m > 1. \qquad (6)$$

For the kagomé lattice we have

$$\xi_{\mathbf{k}} = \sqrt{1 + 8\cos(k_1/2)\cos(k_2/2)\cos([k_1 - k_2]/2)} \qquad (7)$$

with $k_m = \mathbf{k} \cdot \mathbf{a}_m$ and we refer to Ref. 13 for an explicit formula for $\xi_{\mathbf{k}}$ for the pyrochlore lattice.

The three bands of the kagomé lattice consist of one flat band and two dispersing bands. The dispersing bands are identical to the bands of a honeycomb lattice. They are shown together with the density of states per unit cell and spin in Fig. 2. Note, that around the points
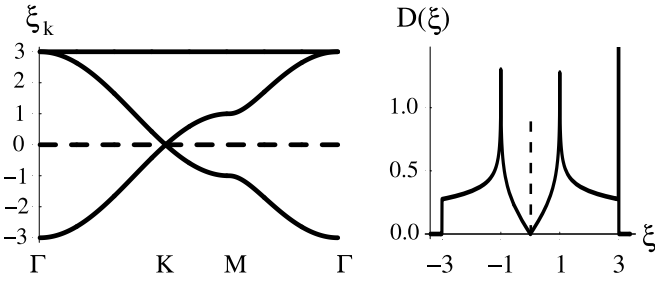

FIG. 2: The kagomé bands and the density of states per unit cell and spin. The energy is measured in units of t.

K and $-$K the dispersion shows a Dirac spectrum, i.e., the bands $\xi_{\mathbf{k}0}$ and $\xi_{\mathbf{k}1}$ touch at these points with linear dispersion. For the given chemical potential the Fermi surface reduces to points at K and $-$K and the density of states vanishes linearly with ξ, i.e., we have $D(\xi) \propto |\xi|$ for small ξ.

The four bands of the pyrochlore lattice consist of two flat bands and two dispersing bands. The dispersing bands are identical to the bands of a diamond lattice. They are shown together with the density of states per unit cell and spin in Fig. 3. Note, that $\xi_{\mathbf{k}}$ vanishes along
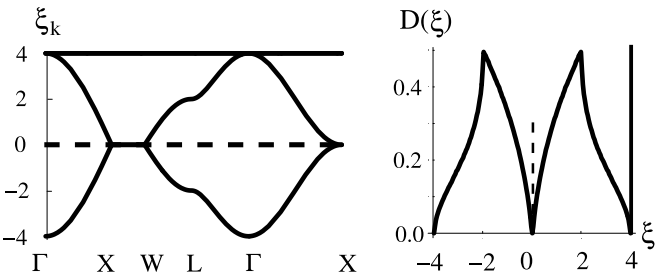

FIG. 3: The pyrochlore bands and the density of states per unit cell and spin. The energy is measured in units of t.

the lines connecting X and W. The density of states also

vanishes linearly at zero up to logarithmic corrections, i.e., we have $D(\xi) \propto |\xi| \log(|\xi|)$ for small ξ.

Systems with this form of the density of states at the Fermi level are neither band-insulators nor normal metals, therefore, they are sometimes called semi-metals or zero-gap semiconductors. Although they have an even number of electrons per unit cell and no fractionally filled bands, they have no energy gap at the Fermi surface. Fermi surface instabilities are suppressed in this situation. There is no Cooper-instability that leads to an obvious breakdown of perturbation theory for arbitrarily small attractive interactions, as the particle-particle polarization function involves the convergent integral $\int d\xi D(\xi)/2|\xi|$ at zero temperature. For the half filled honeycomb lattice it has been shown that the Coulomb interactions lead to non-Fermi liquid behavior and that strong enough Coulomb interactions lead to antiferromagnetic order and to the opening of a charge gap[14–17]. The situation in the kagomé and the pyrochlore lattice at the filling considered here is different. Because the lattices are not at half filling, it is not obvious that even arbitrarily large U would enforce a charge gap (Mott insulator) and an antiferromagnetic order would be hampered by the frustrated topology of the lattice. However, if we consider the triangles (tetrahedra) as the fundamental units of our lattice we obtain the honeycomb (diamond) lattice and the properties of this underlying bipartite lattice will be reflected in the ground state and provide a way to circumvent the frustration effects.

Our goal is to study the electron-electron interactions of the $\hat{H}_{t-J-V}$ Hamiltonian given by

$$\hat{H}_{t-J-V} = \mathcal{P}\hat{H}_0\mathcal{P} + \sum_{\langle ij \rangle} J \, \mathbf{S}_i \cdot \mathbf{S}_j + V n_i n_j, \qquad (8)$$

We will show that both the exchange and the repulsion term favor the bond order wave instability. As the projection operator $\mathcal{P}$ is difficult to handle in analytic calculations, the projection is often approximated by a purely statistical renormalization of the Hamiltonian with Gutzwiller factors[18]. We obtain a renormalized Hamiltonian without constraints given by

$$\hat{H}_{\mathrm{r}} = g_t \hat{H}_0 + \sum_{\langle ij \rangle} J g_J \, \mathbf{S}_i \cdot \mathbf{S}_j + V n_i n_j. \qquad (9)$$

The renormalization is given by the Gutzwiller factors $g_t = 2\delta/(1 + \delta)$ and $g_J = 4/(1 + \delta)^2$ and δ is the hole doping measured from half filling. Note, that the nearest-neighbor repulsion is not renormalized by a statistical factor.

In the following we will determine the critical J and V for spontaneous symmetry-breaking in this model within mean field theory. Superconductivity is a possible way of spontaneous symmetry breaking. As it is an instability in the particle-particle channel, the relation $\xi_{\mathbf{k}} = \xi_{-\mathbf{k}}$, which is ensured by inversion and time reversal symmetry, plays an essential role. Concerning the symmetry of the order parameter, we can restrict ourselves to singlet

pairing in the spin sector, because the nearest neighbor interaction is antiferromagnetic, and to s-wave pairing in the orbital sector, because in this way we obtain a nodeless, even gap-function.

Another possibility of spontaneous symmetry breaking is an instability in the particle-hole channel. Such instabilities tend to occur if a nesting condition of the form $\xi_{\mathbf{k}} = -\xi_{\mathbf{k+q}}$ is fulfilled. In general, this condition is not ensured by basic symmetries and therefore instabilities in the particle-hole channel are much more special than superconducting instabilities. In our case, the relation $\xi_{\mathbf{k}0} = -\xi_{\mathbf{k}1}$ can be considered as perfect nesting with $\mathbf{q} = 0$. Therefore, the relevant question is which one of the two considered instabilities is dominant in our system. In order to answer this question we consider the following single-particle Hamiltonian,

$$\hat{H}_{\text{trial}} = \hat{H}_0 + \Delta_{\text{ph}}\hat{H}_{\text{ph}} + \Delta_{\text{pp}}\hat{H}_{\text{pp}} \qquad (10)$$

where we have introduced the two quadratic Hamiltonians

$$\hat{H}_{\text{ph}} = \sum_{\mathbf{r},\sigma}\sum_{m\neq n}\sum_{\nu=\pm 1} \nu\, c^{\dagger}_{\mathbf{r}+\nu\mathbf{a}_m,\sigma} c_{\mathbf{r}+\nu\mathbf{a}_n,\sigma}, \qquad (11)$$

$$\hat{H}_{\text{pp}} = \sum_{\mathbf{r}}\sum_{m\neq n}\sum_{\nu=\pm 1} (c_{\mathbf{r}+\nu\mathbf{a}_m,\downarrow} c_{\mathbf{r}+\nu\mathbf{a}_n,\uparrow} + \text{h.c.}).$$

The idea is to calculate the expectation value of $\hat{H}_r$ for the ground-state of H_{trial} and to choose the variational parameters Δ_{pp} and Δ_{ph} such that this expectation value is minimized. In terms of the operators that diagonalize $\hat{H}_0$ we can express the pairing operators as

$$\hat{H}_{\text{ph}} = \sum_{\mathbf{k},\sigma} ix_{\mathbf{k}}\gamma^{\dagger}_{\mathbf{k}0\sigma}\gamma_{\mathbf{k}1\sigma} + \text{h.c.}, \qquad (12)$$

$$\hat{H}_{\text{pp}} = \sum_{\mathbf{k},m} \epsilon_{\mathbf{k}m}\gamma_{-\mathbf{k}m\uparrow}\gamma_{\mathbf{k}m\downarrow} + \text{h.c.}.$$

with the relations

$$\xi_{\mathbf{k}m} = \epsilon_{\mathbf{k}m} - \mu, \qquad x^2_{\mathbf{k}} = \xi^2_0 - \xi^2_{\mathbf{k}}. \qquad (13)$$

For small values of Δ_{ph} and Δ_{pp} we can expand the ground-state expectation value of H_r in terms of Δ^2_{pp} and Δ^2_{ph}. Using the Wick theorem, we obtain up to higher order terms

$$\frac{\Delta E}{bN} = \Delta^2_{\text{ph}}I_{\text{ph}}\left[\tilde{t} - \frac{3\tilde{J}}{8}(I_{\text{ph}}-\chi) - \frac{V}{2}(I_{\text{ph}}-\chi)\right] \quad (14)$$

$$+ \Delta^2_{\text{pp}}I_{\text{pp}}\left[\tilde{t} - \frac{3\tilde{J}}{8}(I_{\text{pp}}-\chi) + \frac{V}{2}(I_{\text{pp}}+\chi)\right]$$

where ΔE is the deviation from the ground-state expectation value with $\Delta_{\text{ph}} = \Delta_{\text{pp}} = 0$. N is the number of unit cells, $\tilde{t} = tg_t$, $\tilde{J} = Jg_J$, b is the number of bonds in

the unit cell and

$$\chi = \frac{1}{b}\int_{\xi<0} (-\xi-\mu)D(\xi)d\xi, \qquad (15)$$

$$I_{\text{ph}} = \frac{1}{b}\int_{\xi<0} \frac{\xi^2_0-\xi^2}{|\xi|}D(\xi)d\xi,$$

$$I_{\text{pp}} = \frac{1}{b}\int \frac{(\xi+\mu)^2}{2|\xi|}D(\xi)d\xi.$$

Note that only the density of states enters these formulas because we are restricting ourselves to $\mathbf{q} = 0$ instabilities. The system spontaneously breaks inversion ($U(1)$) symmetry, if the coefficient of Δ^2_{ph} (Δ^2_{pp}) in Eq. (14) changes sign. If we assume that only one of the parameters V and J is nonzero, we obtain the following expressions for the critical values:

$$J^{\text{ph}}_c = \frac{8g_t t}{3g_J(I_{\text{ph}}-\chi)} \qquad V^{\text{ph}}_c = \frac{2g_t t}{(I_{\text{ph}}-\chi)} \quad (16)$$

$$J^{\text{pp}}_c = \frac{8g_t t}{3g_J(I_{\text{pp}}-\chi)} \qquad V^{\text{pp}}_c = \frac{-2g_t t}{(I_{\text{pp}}+\chi)} \quad (17)$$

The numerical values for J_c and V_c are given in TABLE II. One can see, that the tendency for inversion

	d	μ	b	ξ_0	δ	g_t	g_J
K	2	-1	6	3	1/3	1/2	9/4
P	3	-2	12	4	1/2	2/3	16/9

	χ	I_{ph}	I_{pp}	J^{ph}_c	J^{pp}_c	V^{ph}_c	V^{pp}_c
K	0.43	1.08	0.59	0.91	3.58	1.53	-0.98
P	0.32	1.05	0.62	1.36	3.33	1.81	-1.43

TABLE II: The parameters for the kagomé (K) and the pyrochlore (P) lattice. The critical values are given in units of t. The coefficient of Δ_{ph} (bond order wave) in Eq. (14) is negative for $J > J^{\text{ph}}_c$ ($V = 0$) or for *repulsive* $V > V^{\text{ph}}_c$ ($J = 0$). The coefficient of Δ_{pp} (superconductivity) is negative for $J > J^{\text{pp}}_c$ ($V = 0$) or for *attractive* $V < V^{\text{pp}}_c$ ($J = 0$).

symmetry breaking is much stronger than the tendency for superconductivity in both lattices and that both the antiferromagnetic J and the repulsive V support the inversion symmetry breaking. The integral I_{ph} is large because the factor $\xi^2_0 - \xi^2$ takes its maximum at $\xi = 0$ whereas the factor $(\xi + \mu)^2$ in the integral I_{pp} is much smaller for small values of ξ. In other words, superconductivity has the handicap that the potential is proportional to the dispersion $\epsilon_{\mathbf{k}}$, therefore it is small at the Fermi surface and is only finite due to the finite value of μ. The nearest-neighbor repulsion is harmful for Cooper (particle-particle) pairing, as can be seen from Table II. In the particle-hole instability, however, two particles tend to form a singlet on every second triangle (tetrahedron) on the kagomé (pyrochlore) lattice. In this way the singlet is still mobile and keeps $-dt$ of its kinetic energy and at the same time reduces the nearest-neighbor repulsion energy from $4V/3$ ($3V/2$) to V on every second triangle (tetrahedron). On the triangles (tetrahedra)

without a singlet, the expectation value of the nearest-neighbor repulsion is however still $4V/3$ ($3V/2$). In the limit where the kinetic energy is negligible ($t \ll V, J$) also other phases may appear. It is therefore important to emphasize that a finite kinetic energy is necessary to stabilize the bond order wave, because this phase arises due to the interplay between the kinetic and interaction energy.

The limit of large V was recently discussed in the context of LiV$_2$O$_4$ by Yushankhai *et al.* in Ref. 19 for the pyrochlore lattice with $n = 1/2$. The possibility of inversion symmetry breaking was not considered in that study. But if V is of the order of t, the optimization of the kinetic and the repulsion energy can lead to a compromise which breaks the inversion symmetry.

In the bond order wave phase that we found in this section for the kagomé and the pyrochlore lattice, the "up"-triangles (tetrahedra) have a higher expectation value of the kinetic energy than the "down"-triangles (tetrahedra). Furthermore a gap proportional to Δ_{ph} opens at the Fermi surface. Therefore, the system made a transition from a semi-metal to an insulator. This transition is similar to the Peierls metal-insulator transition, where a half filled system lowers spontaneously its crystal symmetry in order to open a gap at the Fermi surface. Phonons or the elasticity of the crystal play a crucial role in the Peierls transition. In our case, as we showed, the transition can be driven by a purely electronic mechanism in an infinitely rigid lattice. In reality, the crystal structure will always relax and in this way additionally enhance the transition.

IV. NUMERICAL RESULTS FOR THE KAGOMÉ LATTICE

In this section we compare the predictions obtained in the preceding sections to numerical results for the kagomé lattice. We will first discuss some exact diagonalization (ED) results for the kagomé lattice at $n = 2/3$, which confirm the BOW clearly and then we will study the dependence of the excitation gaps on the parameter α using the contractor renormalization (CORE) method. In essence the numerical results corroborate the analytical predictions on the presence of a bond order wave instability for the kagomé lattice.

A. Exact Diagonalization results

The analytical arguments presented in Sec. II and Sec. III predict a bond order wave instability at filling $n = 2/3$. In finite, periodic systems this instability can be detected with a correlation function of the bond strength, either of the kinetic term or the exchange term. Here we chose to work with the kinetic term, but the exchange term gives similar results. The correlation function is
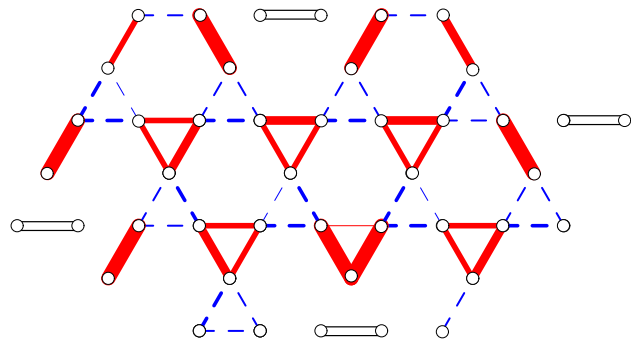

FIG. 4: (Color online) Correlation function of the kinetic energy (Eq. 18) of a 21 sites kagomé sample at $n = 2/3$ and $J/t = 0.4$. The black, empty bonds denote the same reference bond, the red, full bonds negative and the blue, dashed bonds positive correlations. The line strength is proportional to the magnitude of the correlations.

defined as:

$$
\begin{aligned}
C_{\mathrm{Kin}}[(i,j),(k,l)] &= \langle \mathrm{Kin}(i,j)\,\mathrm{Kin}(k,l)\rangle \\
&\quad - \langle \mathrm{Kin}(i,j)\rangle\,\langle \mathrm{Kin}(k,l)\rangle, \quad (18)
\end{aligned}
$$

where

$$
\mathrm{Kin}(i,j) = -\sum_{\sigma} c_{i,\sigma}^{\dagger} c_{j,\sigma} + \mathrm{h.c.}, \quad (19)
$$

and (i,j) and (k,l) denote two different nearest-neighbor bonds of the kagomé lattice, that have no common site. This correlation function has been calculated for all distances in the ground state of a finite kagomé sample with 21 sites, containing 7 holes, at $J/t = 0.4$. The result is plotted in Fig. 4. The reference bond uniquely belongs to a certain class of triangles ("up"-triangle in our case). Based on the theoretical picture one expects the correlation function to be positive for all bonds on the same type of triangles and negative on the others. This is indeed what is seen in Fig. 4. We have also calculated the same quantity for $J/t = 1$ and $J/t = 2$ and the bond order wave correlations (not shown) were becoming even stronger for larger J/t. In this respect the ED calculations confirm the qualitative picture developed above, that the homogeneous $t-J$ model on the kagomé lattice at $n = 2/3$ has an intrinsic instability towards a spontaneous breaking of the inversion symmetry.

B. CORE results

We know from Sec. II A, where we studied the limit of decoupled units, that the system has a finite gap in all sectors for $\alpha = 0$. In this section we show how the gaps of the different sectors of excitations depend on the parameter α.

The CORE algorithm[20–22], which is based on the existence of strong subunits (triangles) that are only weakly coupled, provides a suitable method to perform such a

study. This is certainly true for small values of α where the system is naturally divided into weakly coupled sub-units. For $\alpha = 1$ the CORE algorithm imposes a certain bias, as "up"- and "down"-triangles are not treated on equal footing, however, we have good evidence from ED and from the mean field analysis, that the system itself has a strong tendency to break inversion symmetry spontaneously and therefore we can expect the CORE results to be reliable even for $\alpha = 1$. In fact, we compare the CORE results to the ED results for the smaller clusters, and the good agreement shows that the finite excitation gaps at $\alpha = 1$ are not an artefact of the method.

The CORE method extends the range of tractable sizes of finite clusters, based on a careful selection of relevant low-energy degrees of freedom. In order to apply this algorithm, the lattice has to be divided into blocks; here, we naturally choose the "up"-triangles. A reduced Hilbert space is defined by retaining a certain number of low-lying states on each block. The choice of the states to keep depends also on the quantities to be obtained. While for a ground state calculation fewer states already provide good results, one has to retain usually more states to calculate the excited states. Here we choose to keep the 4 lowest states in the 3-electrons sector, the 7 lowest states with 2 electrons and the 2 lowest states in the 1-electron sector. These states are denoted with an asterix in Table I. This choice leads to a reduction of the local triangle basis from 27 down to 13 states, thus allowing indeed to perform simulations on larger lattices than would be possible by conventional ED.

Then, by computing the exact low-lying eigenstates of two coupled triangles, we calculate the effective interactions at interaction range two for each value of α and we neglect longer range terms. Comparison to ED data on the smaller clusters shows that this approach gives very good results.

The basic excitation gaps of interest in the present problem are the spin gap, the single particle gap and the two particle gap. These are defined as follows:

$$\Delta_{S=1} = E(N_e, 1) - E(N_e, 0), \qquad (20)$$

$$\Delta_{1p} = \frac{1}{2}[E(N_e + 1, 1/2) + E(N_e - 1, 1/2)] - E(N_e, 0), \qquad (21)$$

$$\Delta_{2p} = \frac{1}{2}[E(N_e + 2, 0) + E(N_e - 2, 0)] - E(N_e, 0), \quad (22)$$

where $E(N_e, S^z)$ denotes the ground state energy in the sector with N_e electrons and spin polarization S^z.

We have determined these gaps on kagomé finite size samples at $n = 2/3$ and $J/t = 1$ containing 18 to 27 sites. Two different versions of samples with 18 and 24 sites have been treated (v1 and v2). The results are displayed in Fig. 5. There are two main observations: (1) the gaps do not close for any $\alpha \in [0, 1]$, giving additional evidence for the proposed symmetry breaking; (2) there
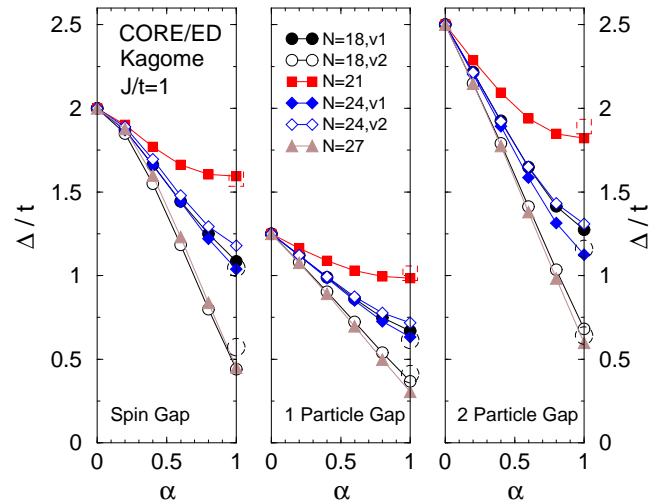

FIG. 5: (Color online) Excitation gaps of the $t-J$ model on the kagomé lattice at $J/t = 1$ as a function of the parameter α, which denotes the ratio of the intertriangle to the intratriangle couplings. The gaps are obtained by the CORE method for different sample sizes (and geometries). For the smaller samples $(18, v1; 18, v2; 21)$ ED data is shown for comparison at $\alpha = 1$.

is a strong dependence of the gap curves on the specific sample. Note that there is no discrepancy between ED and CORE results. The second phenomenon can be understood from the discretization of the finite size Brillouin zones : indeed, the measured gaps directly depend on the distance between the closest point in the Brillouin zone to the corner of the zone, the K-point, which is the point where the gap opens in the mean-field picture (Fig. 2). The 18,v2 and the 27 sites samples both contain this specific point and differ only slightly in the values of the gap. Thus, our numerical data support the claim of a finite gap for all $\alpha \in [0, 1]$. The strong dependence is at the same time also a hint towards a sizable dispersion of the excitations in this system.

V. DMRG AND RG RESULTS FOR THE KAGOMÉ STRIP

In this section we study with two different methods the kagomé strip, shown in Fig. 1 c), as the 1D analogue of the kagomé lattice. This lattice has been introduced in Ref. 23, where it was shown to share some of the peculiar magnetic properties of the 2D kagomé lattice. We report extensive density matrix renormalization group (DMRG) calculations[24], both for the $t-J$ and the Hubbard model. Furthermore, we apply the renormalization group (RG) and the bosonization techniques to the weak coupling Hubbard model. Our results show, that for both, the Hubbard and the $t-J$ model, and irrespective of the coupling strength the BOW phase is realized in the kagomé strip at $n = 2/3$.
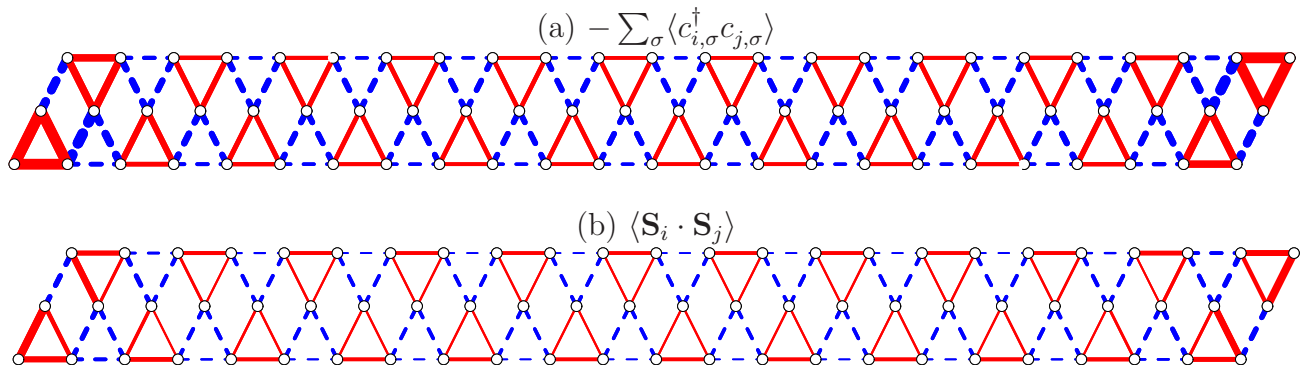
FIG. 6: (Color online) DMRG results for a $L = 24$ kagomé ladder at $J/t = 0.4$ and $n = 2/3$. (a) Local bond strength deviation of the kinetic term. Red, full bonds are stronger (lower in energy) than the average kinetic energy per bond. Blue, dashed bonds are weaker than average bonds. (b) Local bond strength deviation of the exchange term. The color pattern are the same as in the upper panel. The thickness of the bond denotes the deviation from the average value per bond. Note that the pattern of the kinetic and the exchange term are *in phase*.
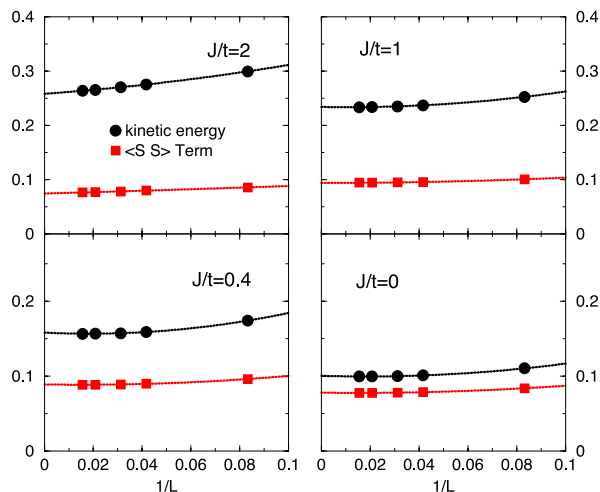
FIG. 7: (Color online) DMRG results for the alternation of the bond strength of the kinetic term and the spin exchange term as a function of inverse system size $1/L$, for different values of J/t.

A. DMRG results

The kagomé strip - being 1D - offers the opportunity to perform DMRG simulations, thus allowing a rather detailed numerical study of large systems. We first discuss the properties of the $t-J$ model at $n = 2/3$ on this lattice, and then make a connection by investigating the Hubbard model at different values of U to the analytical weak-coupling results of the following section. For both models we report numerical evidence for the presence of the bond order wave instability for a large range of interaction strengths.

In contrast to the periodic systems considered above within ED, the DMRG works most efficiently for open boundary conditions (OBC). In the present context this has the additional advantage that for even length L of

the strip only one of the two degenerate ground states is favored, and we can directly measure the local bond strength. For the purpose of illustration we show the local bond strengths for a system of $L = 24$ in Fig. 6. The upper panel shows the difference of the local kinetic energy with respect to the average, while the lower panel shows the local expectation value of the spin exchange term, using the same convention.

The calculated pattern resembles the schematic picture drawn in Fig 1 c). In order to address the behavior in the thermodynamic limit we measure the bond strength alternation, i.e., the difference between the expectation values of the operators $\text{Kin}(i,j)$ and $\mathbf{S}_i \cdot \mathbf{S}_j$ in the middle of the system for different lengths L and values of J/t. The scaling of these quantities is shown in Fig. 7. The finite size corrections are rather small and all the order parameters extrapolate to finite values, irrespective of the value of J/t. Note that even for the case $J/t = 0$ there is both a finite alternation of the kinetic energy *and* the magnetic exchange term. The alternation of the magnetic exchange energy is roughly the same for all values of J/t. The alternation of the kinetic energy however is increased with growing J/t ratio.

Next we address the question of the excitation gaps in the symmetry broken phase. The theoretical picture predicts an insulating state with a finite gap to all excitations above the two-fold degenerate ground state. We calculate the single particle charge gap and the spin gap defined in equations (21) and (20), respectively. The calculated gaps are shown in Fig. 8. The finite size gaps are extrapolated to $L = \infty$ with a simple quadratic fit. All gaps extrapolate to a finite value, in agreement with the predictions. The charge gap more or less follows the increase of the alternation of the kinetic energy shown in Fig. 7, i.e., the gap is roughly multiplied by a factor three going from $J/t = 0$ to 2. The behavior of the spin gap is mainly driven by the fact that it scales with J/t. Note that even in the case $J/t = 0$ the spin gaps seem to remain finite. It will be an interesting question
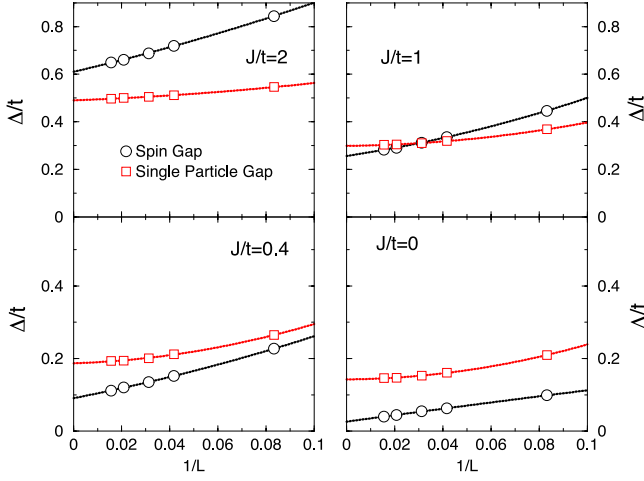
FIG. 8: (Color online) DMRG results for the spin gap and single particle gap for $J/t = 0, 0.4, 1, 2$, as a function of inverse system size $1/L$.
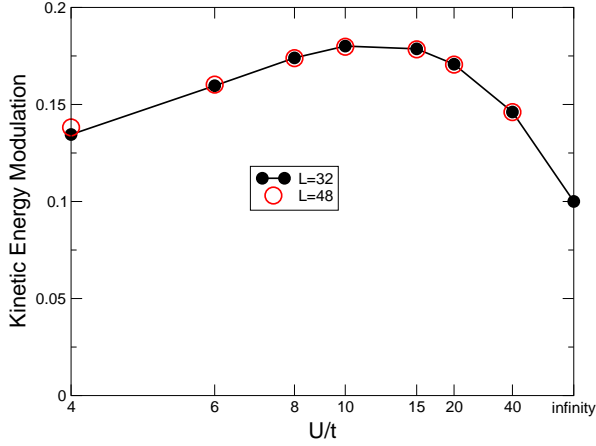

FIG. 9: (Color online) DMRG results for the kinetic energy alternation for Hubbard kagomé strips at $n = 2/3$ of length $L = 32$ and $L = 48$. The modulation is non-monotonous as a function of U/t and shows a maximum around $U/t \approx 10 \sim 15$.

to characterize the precise nature of the charge and spin excitations. This will be left for a future study.

The weak coupling RG calculations in the following section are performed for Hubbard onsite interactions. Although we expect the behavior of the $t-J$ model and the Hubbard model at large U to be similar, we have explicitly calculated the alternation of the kinetic energy for the Hubbard model as a function of U/t. The results displayed in Fig. 9 show that this quantity has a maximum around $U/t \approx 10 \sim 15$, and interpolates between the exponentially small order parameter at weak U/t and the result for the $t-J$ model at $J = 0$, which corresponds to $U = \infty$. These results therefore suggest that for the particular case of the kagomé strip the weak-coupling phase is adiabatically connected to the strong coupling limit.
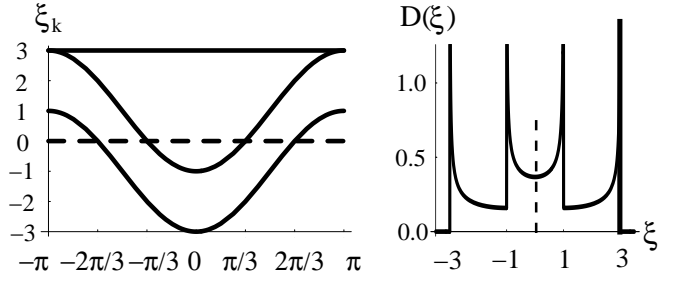

FIG. 10: The kagomé strip bands and the density of states per unit cell and spin. The energy is measured in units of t.

B. Weak-coupling discussion

We consider in this section the weak-coupling Hubbard model with the interaction

$$H_{\text{Int}} = U \sum_{\mathbf{r}} c^{\dagger}_{\mathbf{r},\uparrow} c^{\dagger}_{\mathbf{r},\downarrow} c_{\mathbf{r},\downarrow} c_{\mathbf{r},\uparrow}, \qquad (23)$$

on the 1D kagomé strip. We map this weak local Coulomb repulsion on the original kagomé strip on an effective interaction for the underlying half filled two-leg ladder. We will show in the following that for the one-dimensional kagomé strip, applying the RG and bosonization techniques that were developed for the half filled two-leg ladder, we find in fact a charge density wave (CDW) instability in the effective model for the two-leg ladder which corresponds to a BOW instability on the kagomé strip.

The tight-binding bands of the kagomé strip with $\mu = -t$ are shown in Fig. 10. The dispersing bands are the same as the bands of a two-leg ladder. The flat band originates from states that are trapped within one rhombus. The density of states has square-root singularities at $\pm t, \pm 3t$ and a delta-peak at $3t$. The Fermi surface is given by the 4 points $\pm k_{\text{F1}}$ and $\pm k_{\text{F2}}$, where $k_{\text{F1}} = \pi/3$ and $k_{\text{F2}} = 2\pi/3$. There is a finite density of states at the Fermi surface. The kagomé strip can be viewed as a kagomé lattice tube, i.e., a kagomé lattice with finite width and periodic boundary conditions. In order to see that the bands in Fig. 10 are in fact a cut through the kagomé dispersion shown in Fig. 2, one has to shift one of the dispersing bands by π. This difference arises because our notation is chosen to emphasize the similarities of the kagomé strip to the two-leg ladder.

In contrast to the kagomé and the pyrochlore lattice, the density of states at the Fermi surface is finite for the kagomé strip and we therefore expect qualitative changes in this 1D system even for weak interactions. We perform a weak-coupling RG and bosonization analysis for the kagomé strip, and we show that the bond order wave instability is already present for arbitrary weak coupling. In this section we will only present the results of this analysis and refer to Appendix A 1 for further details.

We derive an effective interaction for the two-leg ladder, that corresponds in weak coupling to the local

Coulomb repulsion on the kagomé strip (23). In this derivation we can drop terms that involve the high energy states of the flat band and focus on the states in the dispersing bands. We denote the annihilation operator of these states by $\gamma_{\mathbf{k},\sigma} = \gamma_{k,i,\sigma}$ where k is the momentum along the strip and $i \in \{1, 2\}$ is the band index. If we rewrite the Hamiltonian H_{Int} in terms of these new operators we obtain the interaction.

$$H_{\mathrm{Int}} \rightarrow \frac{U}{L} \sideset{}{'}\sum_{\mathbf{k}_1 \ldots \mathbf{k}_4} g_{\mathbf{k}_1 \ldots \mathbf{k}_4} \, \gamma^\dagger_{\mathbf{k}_1,\uparrow} \gamma^\dagger_{\mathbf{k}_2,\downarrow} \gamma_{\mathbf{k}_3,\downarrow} \gamma_{\mathbf{k}_4,\uparrow}, \quad (24)$$

where the prime over the sum restricts the sum to momentum conserving $\mathbf{k}$-values. For weak interaction we can replace $\mathbf{k}_l$ in $g_{\mathbf{k}_1 \ldots \mathbf{k}_4}$ by $(k_{\mathrm{F}i_l}, i_l)$ and we obtain the simple expression

$$g_{\mathbf{k}_1 \ldots \mathbf{k}_4} = e^{-i\frac{q}{2}} (\delta_{i_1 i_2}\delta_{i_3 i_4} + \delta_{i_1 i_3}\delta_{i_2 i_4} + \delta_{i_1 i_4}\delta_{i_2 i_3})/6, \; (25)$$

where $q = k_1 + k_2 - k_3 - k_4$.

The effective interaction (24) can now be expressed in terms of left and right moving currents and in this way we find the initial values for the RG equations of the two-leg ladder. The integration of the RG equations with these initial values converges to an analytic solution that was identified by bosonization techniques as a charge density wave solution[25]. This means that the operator

$$O_{\mathrm{CDW}} = \frac{1}{L} \sum_{k,\sigma} \gamma^\dagger_{k,1,\sigma}\gamma_{k+\pi,2,\sigma} + \gamma^\dagger_{k+\pi,2,\sigma}\gamma_{k,1,\sigma} \quad (26)$$

acquires a finite value. The bond order wave order-parameter on the kagomé strip is given by the expectation value of an operator O_{BOW}.

The operators O_{CDW} and O_{BOW} transform identically under all symmetries of the system and, therefore, they describe the same phase.

In addition, O_{CDW} is the effective operator on the two-leg ladder for O_{BOW}, i.e., if one does the same substitutions as we did for deriving Eq. (24) one sees that $O_{\mathrm{BOW}} \rightarrow O_{\mathrm{CDW}}$, if one chooses the right prefactor in the definition of O_{BOW}.

We have shown that the bond order wave instability that is expected to occur at rather strong interactions according to the arguments of the preceding sections, is in fact already present in weak coupling for the one-dimensional kagomé strip. Together with the DMRG results of the preceding section we provide convincing evidence, that the BOW phase on the kagomé strip is present both in the Hubbard model for all values of U and in the $t-J$ model.

VI. CONCLUSIONS

In summary we have studied the occurrence of a bond order wave instability in several bisimplex lattices. We provided evidence that this instability occurs quite generally in these lattices at the fractional filling of one electron per simplex (two electrons per "up"-simplex), if the correlations – i.e., antiferromagnetic nearest-neighbor exchange and/or nearest-neighbor repulsion – are strong enough.

In weak-coupling the physical properties of the system are dominated by the dimensionality of the lattice, by its fermiology and by the density of states at the Fermi energy. We show that in the intermediate coupling regime, where the kinetic and the interaction energies are comparable, at the filling with two electrons per "up"-simplex, the physical properties of these highly frustrated lattices are dominated by local states on the simplex. The bipartite and corner-sharing arrangement of the simplices allows the creation of isolated or only weakly interacting simplices with low energy by spontaneously breaking inversion or translational symmetry. This knowledge provides a good starting point for series expansions or further CORE calculations.

The magnetic interaction and the chosen sign of the dispersion leads to a tendency to form nearest-neighbor singlets and nearest-neighbor repulsion leads to a tendency to avoid configurations with more than two electrons per simplex. If the underlying lattice is bipartite the system finds a way to satisfy both tendencies simultaneously by localizing singlets on every second simplex. This localization leads only to a partial loss of the kinetic energy, because the singlets can still delocalize within the simplex. It is the cooperation between the kinetic and the interaction energy which stabilizes the bond order wave state. Note, that the bond order wave instability does not lead to an inhomogeneous charge distribution on the lattice.

The bond order wave states, which we find on the different lattices, provide a natural generalization of the well-known valence bond solid states (e.g. dimerized phases, plaquette phases) found in many frustrated spin models to situations away from half filling where a description in terms of spin variables only breaks down. The density is still a rational fraction, but $n = 2/3$ in the kagomé and kagomé strip case while $n = 1/2$ in the pyrochlore and the checkerboard case. Approximately these states are direct products of singlets on triangles or tetrahedra, similar to the conventional picture of a dimerized phase. In contrast to the phases at $n = 1$ however, the present instability involves a cooperative effect of both magnetic exchange *and* kinetic energy.

An interesting task is to study the properties of a lightly doped bond order wave phase. It can be assumed that the bond order wave order parameter decreases rather quickly with doping. However, it is conceivable that away from the commensurate filling the bond order wave order parameter coexists with a small superconducting order parameter. This phase would at the same time break lattice symmetries and the $U(1)$ gauge symmetry and would be therefore similar to a supersolid. A closer investigation of these issues has however be left for

further studies.

In general, we conclude that the bond order wave instability occurs quite generally in bisimplex lattices and for physically reasonable models and interaction parameters. We show that doping frustrated spin models can lead to new phases. Our study may also be a step towards the understanding of the interplay of frustrated magnetic fluctuations and itinerant charge carriers, which could play a role for example in the unconventional heavy Fermion material LiV_2O_4[7] or in Na_xCoO_2.

APPENDIX A: RG ANALYSIS

1. kagomé strip

The tight-binding Hamiltonian for the kagomé strip with periodic boundary conditions is given by

$$\hat{H}_0 = -t \sum_{r=1}^{L} \sum_{\nu=\pm 1} \sum_{\sigma} \left[c_{r,\nu,\sigma}^\dagger c_{r+\nu,\nu,\sigma} + \right. \tag{A1}$$
$$\left. + c_{r,0,\sigma}^\dagger (c_{r,\nu,\sigma} + c_{r+\nu,\nu,\sigma}) + \text{h.c.} \right] - \mu \hat{N},$$

where $\sigma \in \{\uparrow, \downarrow\}$ are the spin indices and $\hat{N}$ is the number operator. The chemical potential, μ, will be fixed to $-t = -1$ in the following. It is convenient to introduce Fourier transformed operators

$$c_{r,x} = \frac{1}{\sqrt{L}} \sum_k e^{ik(r-\frac{x}{2})} c_{k,x} \qquad x \in \{\pm 1, 0\}, \tag{A2}$$

where the k-sum runs over the L k-values in $[-\pi, \pi)$. We can write this Hamiltonian in a diagonal form

$$\hat{H}_0 = \sum_k \sum_{l=1}^3 \sum_\sigma \xi_{k,l} \, \gamma_{k,l,\sigma}^\dagger \gamma_{k,l,\sigma},$$

and obtain the energies

$$\xi_{k,1} = 1 - 2\cos(k), \ \xi_{k,2} = -1 - 2\cos(k), \ \xi_{k,3} = 3. \tag{A3}$$

and the operators

$$\begin{bmatrix} \gamma_{k,1,\sigma} \\ \gamma_{k,2,\sigma} \\ \gamma_{k,3,\sigma} \end{bmatrix} = \frac{1}{\sqrt{2}\beta_k} \begin{bmatrix} \beta_k & 0 & -\beta_k \\ \alpha_k & \sqrt{2} & \alpha_k \\ 1 & -\sqrt{2}\alpha_k & 1 \end{bmatrix} \begin{bmatrix} c_{k,-1} \\ c_{k,0} \\ c_{k,+1} \end{bmatrix} \tag{A4}$$

with $\alpha_k = \sqrt{2}\cos(k/2)$ and $\beta_k = \sqrt{1 + \alpha_k^2}$ and $k \in [-\pi, \pi)$.

The local Coulomb interaction introduced in Eq. (23) can be written as

$$H_{\text{Int}} = \frac{U}{L} \sum_{k_1\ldots k_4}' \sum_{x=-1}^{1} e^{-i\frac{xq}{2}} c_{k_1,x,\uparrow}^\dagger c_{k_2,x,\downarrow}^\dagger c_{k_3,x,\downarrow} c_{k_4,x,\uparrow}. \tag{A5}$$

The sum over the momenta $k_1 \ldots k_4$ is restricted, such that $q = k_1 + k_2 - k_3 - k_4$ is a multiple of 2π. Note, that the appearing phase factor is important to determine the sign of the Umklapp scattering processes correctly. We obtain the effective low-energy Hamiltonian (24) from Eq. (A5) by doing the substitutions

$$c_{k,\pm,\sigma} \rightarrow \mp \frac{1}{\sqrt{2}} \gamma_{k,1,\sigma} + \frac{1}{\sqrt{6}} \gamma_{k,2,\sigma} \tag{A6}$$

$$c_{k,0,\sigma} \rightarrow \sqrt{\frac{2}{3}} \gamma_{k,2,\sigma}.$$

These substitutions rules are obtained from Eq. (A4) if we set $k = k_{F1}$ in the first row and $k = k_{F2}$ in the second row and drop the third row in the matrix of the transformation.

In this way we can map the weak-coupling Hubbard model on the kagomé strip on an effective weak-coupling model on the two-leg ladder. The problem of a weak-coupling two-leg ladder has been extensively studied by renormalization-group and bosonization techniques[25–27]. We will adopt here the notation of Lin *et al.* in Ref. 25. A general weak interaction can be conveniently expressed in terms of left and right moving currents. Dropping purely chiral terms the momentum-conserving four fermion interactions can be written as

$$\mathcal{H}^{(1)} = b_{ij}^\rho J_{Rij} J_{Lij} - b_{ij}^\sigma \mathbf{J}_{Rij} \cdot \mathbf{J}_{Lij} \tag{A7}$$
$$+ f_{ij}^\rho J_{Rii} J_{Ljj} - f_{ij}^\sigma \mathbf{J}_{Rii} \cdot \mathbf{J}_{Ljj}.$$

To avoid double counting we set $f_{ii} = 0$. Furthermore, the symmetry relations $f_{12} = f_{21}$ (parity), $b_{12} = b_{21}$ (hermicity), and $b_{11} = b_{22}$ (only at half filling) hold. We have therefore six independent coefficients. For our interaction we find the values

$$4b_{11}^\rho = b_{11}^\sigma = U, \quad 4b_{12}^\rho = b_{12}^\sigma = \frac{U}{3}, \quad 4f_{12}^\rho = f_{12}^\sigma = \frac{U}{3}.$$

In addition we have Umklapp terms given by

$$\mathcal{H}^{(2)} = u_{ij}^\rho I_{Rij}^\dagger I_{L\bar{i}\bar{j}} - u_{ij}^\sigma \mathbf{I}_{Rij}^\dagger \cdot \mathbf{I}_{L\bar{i}\bar{j}} + \text{h.c.}$$

with $u_{ii}^\sigma = 0$, $u_{11}^\rho = u_{22}^\sigma$ and $u_{12}^\rho = u_{21}^\sigma$ and $u_{12}^\sigma = u_{21}^\sigma$. Here we have the values

$$u_{12}^\sigma = 0, \quad u_{12}^\rho = -\frac{U}{12}, \quad u_{11}^\rho = -\frac{U}{24}.$$

Integrating the RG equations with these initial values shows that the solution converges to the analytic solution

of the RG equation where all coupling constants except for b_{11}^σ and b_{11}^ρ diverge with fixed ratios given by

$$f_{12}^\rho = -\frac{1}{4}f_{12}^\sigma = b_{12}^\rho = -\frac{1}{4}b_{12}^\sigma \qquad (A8)$$
$$= \frac{1}{2}u_{12}^\sigma = -2u_{12}^\rho = -2u_{11}^\rho = g > 0.$$

This solution was identified by bosonization techniques as a charge density wave solution (CDW) solution.

[1] Y. Imai, N. Kawakami, and H. Tsunetsugu, Phys. Rev. B **68**, 195103 (2003).

[2] A. Läuchli and D. Poilblanc, Phys. Rev. Lett. **92**, 236404 (2004).

[3] D. Poilblanc, Phys. Rev. Lett. **93**, 197204 (2004).

[4] N. Bulut, W. Koshibae, and S. Maekawa, Phys. Rev. Lett. **95**, 037001 (2005).

[5] E. Runge and P. Fulde, Phys. Rev. B **70**, 245113 (2004).

[6] S. Fujimoto, Phys. Rev. B **64**, 085102 (2001); Phys. Rev. Lett. **89**, 226402 (2002).

[7] S. Kondo, D.C. Johnston, C.A. Swenson et al., Phys. Rev. Lett. **78**, 3729 (1997); S.-H. Lee, Y. Qiu, C. Broholm, Y. Ueda, and J. J. Rush, Phys. Rev. Lett. **86**, 5554 (2001).

[8] L. Santos, M. A. Baranov, J. I. Cirac, H.-U. Everts, H. Fehrmann, and M. Lewenstein, Phys. Rev. Lett. **93**, 030601 (2004).

[9] B. Damski, H.-U. Everts, A. Honecker, H. Fehrmann, L. Santos, and M. Lewenstein, Phys. Rev. Lett. **95**, 060403 (2005).

[10] C.L. Henley, Can. J. Phys. **79**, 1307 (2001).

[11] T. Koretsune, and M. Ogata, J. Phys. Soc. Jpn. **72**, 2437 (2003).

[12] R. Moessner, S. Sondhi, and M. Goerbig, Phys. Rev. B **73**, 094430 (2006).

[13] M. Isoda and S. Mori, J. Phys. Soc. Jpn. **69**, 1509 (2000).

[14] S. Sorella and E. Tosatti, Europhys. Lett. **19**, 699 (1992).

[15] L. M. Martelo, M. Dzierzawa, L. Siffert, D. Baeriswil, Z. Phys. B **103**, 335 (1997).

[16] J. González, F. Guinea, M.A.H. Vozmediano, Nucl. Phys. B **424**, 595 (1994).

[17] J. González, F. Guinea, M.A.H. Vozmediano, Phys. Rev. B **63**, 134421 (2001).

[18] F. C. Zhang, C. Gros, T. M. Rice, and H. Shiba, Supercond. Sci. Technol. **1**, 36 (1988).

[19] V. Yushankhai, P. Fulde, and P. Thalmeier, Phys. Rev. B **71**, 245108 (2005).

[20] C. J. Morningstar, and M. Weinstein, Phys. Rev. D, **54**, 4131 (1996).

[21] S. Capponi, A. Läuchli, and M. Mambrini, Phys. Rev. B, **70**, 104424 (2004).

[22] E. Altman and A. Auerbach, Phys. Rev. B **65**, 104508 (2002); E. Berg, E. Altman, and A. Auerbach, Phys. Rev. Lett. **90**, 147204 (2003); R. Budnik and A. Auerbach, Phys. Rev. Lett. **93**, 187205 (2004).

[23] Ch. Waldtmann, H. Kreutzmann, U. Schollwöck, K. Maisinger, and H.-U. Everts, Phys. Rev. B **62**, 9472 (2000).

[24] S.R. White, Phys. Rev. Lett. **69**, 2863 (1992).

[25] H.-H. Lin, L. Balents, and M.P.A. Fisher, Phys. Rev. B **58**, 1794 (1998).

[26] J. O. Fjærestad and J. B. Marston, Phys. Rev. B **65** 125106 (2002).

[27] M. Tsuchiizu and A. Furusaki, Phys. Rev. B **66**, 245106 (2002).